RSC Advances

PAPER

View Article Online
View Journal | View Issue

Open Access Article. Published on 04 December 2024. Downloaded on 10/25/2025 4:52:21 AM.
This article is licensed under a Creative Commons Attribution-NonCommercial 3.0 Unported Licence.

Check for updates

Cite this: *RSC Adv.*, 2024, **14**, 38364

The novel quinoline derivative SKA-346 as a $K_{Ca}3.1$ channel selective activator†

Brandon Han Siang Wong,[ab] Heesung Shim,[c] Stephanie Shee Min Goay,[ad] Seow Theng Ong,[ad] Nur Ayuni Binte Muhammad Taib,[e] Kelila Xin Ye Chai,[e] Kerry Lim,[e] Dachuan Huang,[ef] Choon Kiat Ong,[ef] Thamil Selvan Vaiyapuri,[g] Yeong Cheng Cheah,[h] Yulan Wang,[h] Heike Wulff,[j] Richard D. Webster,[k] Vishalkumar G. Shelat[ai] and Navin Kumar Verma *[a]

Received 12th October 2024
Accepted 17th November 2024

DOI: 10.1039/d4ra07330d

rsc.li/rsc-advances

The calcium-activated $K_{Ca}3.1$ channel plays a crucial role in T-cell immune response. Genetic manipulation of T-cells to upregulate the expression of K^+ channels has been shown to boost T-cell cytotoxicity in cancer. Here, we aimed to identify and characterize an activator that would augment $K_{Ca}3.1$ currents without affecting other channels. We synthesized five quinoline derivatives and used electrophysiology to screen them on $K_{Ca}3.1$ and a panel of 14 other ion channels. One quinoline derivative, **SKA-346**, activated $K_{Ca}3.1$ with an EC_{50} of 1.9 μM and showed selectivity against the other channels. *In silico* analysis using RosettaLigand and GLIDE demonstrated a well-converged pose of **SKA-346** in a binding pocket at the interface between the calmodulin N-lobe and the $S_{45}A$ helix in the S4–S5 linker of the $K_{Ca}3.1$ channel. **SKA-346** (30 mg kg^{-1}), tolerated by mice after intra-peritoneal administration, exhibited a peak plasma concentration of 6.29 μg mL^{-1} (29.2 μM) at 15 min and a circulating half-life ($t_{1/2}$) of 2.8 h. **SKA-346** could serve as a template for the development of more potent $K_{Ca}3.1$ activators to enhance T-cell cytotoxicity in cancer.

1 Introduction

Potassium (K^+) channels play a key role in the immune function. Human T-cells use the voltage-dependent $K_V1.3$ channel and the intermediate-conductance Ca^{2+}-activated $K_{Ca}3.1$ channel to regulate membrane potential and K^+ efflux.[1] Following activation, both naïve and central memory T-cells transcriptionally up-regulate $K_{Ca}3.1$ channels (<20 channels per cell to >500 channels per cell) without a change in $K_V1.3$ expression, while effector memory T-cells upregulate $K_V1.3$ channels (200 channels per cell to 1500 channels per cell) without altering $K_{Ca}3.1$ expression. Consequently, $K_{Ca}3.1$ plays an important functional role in activated naïve and central memory T-cells, while $K_V1.3$ modulates the function of effector memory T-cells.[2] $K_{Ca}3.1$ channels are also expressed in other cell types, including macrophages,[3] mast cells,[4] microglia,[5] fibroblasts,[6] dedifferentiated proliferating smooth muscles,[7,8] airway epithelium[9] and vascular endothelium.[10]

Unlike large-conductance Ca^{2+}-activated K^+ channels which directly bind Ca^{2+}, intracellular Ca^{2+} interacts indirectly with $K_{Ca}3.1$,[11] through calmodulin, constitutively bound to the C-terminal region of $K_{Ca}3.1$. Binding of Ca^{2+} to channel-bound calmodulin induces a conformational change that opens the channel pore and increases K^+ efflux.[12] K^+ efflux results in hyperpolarization of the membrane potential, which provides the electrochemical gradient needed to drive Ca^{2+} influx into the cell. Ca^{2+}-dependent cellular processes,[13] important for T-cell activation and effector functions involving proliferation, differentiation, and migration, are thereby regulated by the dynamic and precise control of the membrane potential.[14–16]

The death of cancer cells in tumours is associated with poor patient prognosis.[17] Dying tumour cells release K^+, the main intracellular cation, which accumulates in the tumour

[a]Lee Kong Chian School of Medicine, Nanyang Technological University Singapore, Singapore. E-mail: nkverma@ntu.edu.sg
[b]Interdisciplinary Graduate Programme, NTU Institute for Health Technologies (HealthTech NTU), Nanyang Technological University Singapore, Singapore
[c]Physical and Life Sciences, Lawrence Livermore National Laboratory, Livermore, CA, USA
[d]LKCMedicine-ICE Collaborative Platform, Lee Kong Chian School of Medicine, Nanyang Technological University Singapore, Singapore
[e]Lymphoma Translational Research Laboratory, Division of Cellular and Molecular Research, National Cancer Centre, Singapore
[f]Duke-NUS Medical School, Singapore
[g]MMD Lab, Institute of Molecular and Cell Biology, A*STAR, Singapore
[h]Singapore Phenome Center, Lee Kong Chian School of Medicine, Nanyang Technological University Singapore, Singapore
[i]Department of General Surgery, Tan Tock Seng Hospital, Singapore
[j]Department of Pharmacology, University of California Davis, CA, USA
[k]School of Chemistry, Chemical Engineering and Biotechnology, Nanyang Technological University Singapore, Singapore

† Electronic supplementary information (ESI) available. See DOI: https://doi.org/10.1039/d4ra07330d

© 2024 The Author(s). Published by the Royal Society of Chemistry

Open Access Article. Published on 04 December 2024. Downloaded on 10/25/2025 4:52:21 AM. This article is licensed under a Creative Commons Attribution-NonCommercial 3.0 Unported Licence.

microenvironment (TME), reaching 5–10 times the levels encountered by T-cells in the bloodstream. T-cells in the TME exposed to the K^+-rich fluid accumulate K^+ intracellularly due to greater entry through 'pump' or 'leak' channels than exit through $K_{Ca}3.1$ and $K_V1.3$ K^+ channels.[18,19] The increased intracellular K^+ suppresses genes involved in a myriad of pathways in T-cells, nutrient consumption and metabolic changes are altered, the transition of T-cells from the resting to the tumour-killing effector stage is inhibited, and the transition to regulatory T-cells that dampen immune responses is promoted. These alterations occur without affecting the viability of T-cells.[18,19] Overexpression of $K_V1.3$ or $K_{Ca}3.1$ K^+ channels in T-cells rescues T-cells from the immunosuppressive effects of the K^+-rich TME.[18] Moreover, defects in $K_{Ca}3.1$ activity hinder T-cell recruitment in the adenosine-rich TME, thereby promoting tumour immune escape.[14,20] Pharmacological activation of the $K_{Ca}3.1$ channels in T-cells thus represents a promising approach to boost anti-tumour T-cell immunity within the TME.[21]

While $K_{Ca}3.1$ inhibitors are in pre-clinical development to dampen T-cell hyperactivation in autoimmune diseases, there is limited information on $K_{Ca}3.1$ channel activators. A previously developed $K_{Ca}3.1$ activator, SKA-31, potently augmented $K_{Ca}3.1$ activity and lowered blood pressure in experimental mice,[22] but it lacked selectivity over closely related small-conductance Ca^{2+}-activated $K_{Ca}2$ channels.[23] Here, we synthesized a panel of five compounds structurally related to SKA-31 and demonstrate that one analogue, **SKA-346**, effectively activates $K_{Ca}3.1$ and exhibits selectivity for $K_{Ca}3.1$ over related channels. We further show *in vivo* tolerability, pharmacokinetic profiles, and tissue distribution of **SKA-346** in mice. These findings will be helpful for evaluating **SKA-346** as a novel therapy for conditions requiring specific activation of the $K_{Ca}3.1$ channel such as alleviating the immunosuppressive effects on tumour-infiltrating lymphocytes in the necrotic microenvironment of solid tumours.

2 Results and discussion

2.1. Chemistry of quinoline derivatives

The synthesis steps of the five quinoline derivative compounds (i) 5-methyl-[1,3]thiazolo[4,5-*f*]quinolin-2-amine (**SKA-346**), (ii) 8-(trifluoromethyl)thiazolo[4,5-*f*]quinolin-2-amine (**NKV-101**), (iii) 5-methyl-8-(trifluoromethyl)thiazolo[4,5-*f*]quinolin-2-amine (**NKV-102**), (iv) 5-fluoro-[1,3]thiazolo[4,5-*f*]quinolin-2-amine (**NKV-103**), and (v) 5-(trifluoromethyl)thiazolo[4,5-*f*]quinolin-2-amine (**NKV-104**) are provided in Scheme 1. Final products of all the five quinoline derivatives were confirmed by proton nuclear magnetic resonance spectroscopy (^{1}H NMR) and liquid chromatography-mass spectrometry (LC-MS) (ESI Fig. 1–5†).

2.1.1. Synthesis of SKA-346. The synthesis procedure of **SKA-346** is outlined in Scheme 1A. Briefly, 5-amino-8-methylquinoline (500 mg) (**1**) and potassium thiocyanate (KSCN, 3.5 mmol) were dissolved in glacial acetic acid at room temperature. In a dropwise manner, liquid bromine (Br_2, 1.2–1.5 equivalent) in glacial acetic acid was added and the reaction mixture was stirred for 2 h. Subsequently, solids were filtered and washed with glacial acetic acid followed by H_2O. The filtrate was diluted with H_2O (100 mL) and the pH was adjusted in the range of 7.0–7.5 prior to cooling in the refrigerator overnight for product precipitation. Finally, the product was filtered and washed with cold H_2O before drying under vacuum. The product was isolated as brownish powder and confirmed by ^{1}H NMR and LC-MS (110 mg, 16%); m.p. = 259 °C (CAS 1082847-64-0). ^{1}H NMR (800 MHz, DMSO-d_6): δ = 8.88 (dd, J = 4.1, 1.9 Hz, 1H), 8.66 (dd, J = 8.3, 1.9 Hz, 1H), 7.90 (t, J = 1.2 Hz, 1H), 7.63 (s, 2H), 7.54 (dd, J = 8.2, 4.1 Hz, 1H), 2.69 (d, J = 1.1 Hz, 3H). ^{13}C NMR (201 MHz, DMSO-d_6): δ = 168.19, 148.72, 146.89, 146.02, 132.22, 129.13, 125.57, 122.45, 121.20, 121.14, 39.93, 18.38 (ESI Fig. 1†).

2.1.2. Synthesis of NKV-101. The 5-steps synthesis process (Scheme 1B) was initiated using 5-bromo-3-(trifluoromethyl) quinoline (0.30 g, 1.086 mmol) (**2**). In a stirred solution with toluene (10 mL), diphenylmethanimine ($Ph_2C{=}NH$) (1 equivalent, 0.19 g, 1.086 mmol) and cesium carbonate (Cs_2CO_3) (2 equivalent, 0.70 g, 2.173 mmol) were added. The reaction mixture was degassed with argon for 10 min prior to the addition of palladium acetate ($Pd(OAc)_2$) (0.1 equivalent, 0.04 g, 0.217 mmol) and Xantphos (0.2 equivalent, 0.0031 g, 0.005 mmol) and subsequently stirred at 120 °C for 16 h. After completion (monitored by thin layer chromatography, TLC), the mixture was quenched with ice-cold H_2O (10 mL), extracted with ethyl acetate (EtOAc) (2 × 50 mL) and washed with brine (10 mL). The organic layer was then dried over anhydrous sodium sulfate (Na_2SO_4) and concentrated under reduced pressure. The crude was then purified by combi-flash column chromatography (70% EtOAc/heptane) to afford 1,1-diphenyl-*N*-(3-(trifluoromethyl)quinolin-5-yl)methanimine (**3**; 0.20 g, 0.531 mmol, 48.89%). Compound **3** (0.03 g, 0.079 mmol), in a stirred solution of HCl (1 mL) at 0 °C, was stirred at room temperature for 2 h. Upon completion (monitored by TLC), the reaction mixture was quenched with ice-cold H_2O (5 mL) and extracted with EtOAc (2 × 10 mL). The aqueous layer was basified with saturated sodium bicarbonate ($NaHCO_3$; pH 8.0), washed with brine, dried over anhydrous Na_2SO_4 and concentrated under reduced pressure to afford 3-(trifluoromethyl) quinolin-5-amine hydrochloride (**4**; 0.015 g, 0.070 mmol, 88.70%). Benzoyl isothiocyanate (PhCONCS) (2 equivalent, 0.19 g, 1.206 mmol) was then added to **4** (0.15 g, 0.603 mmol) in a stirred solution of acetone (CH_3COCH_3; 12 mL). Sequentially, the reaction mixture was stirred at room temperature for 1 h. After completion (monitored by TLC), the mixture was diluted with EtOAc and H_2O. The organic layer was separated, washed with brine, and concentrated under reduced pressure. The crude was purified by combi-flash column chromatography (40–60% EtOAc/hexane) to afford *N*-((3-(trifluoromethyl)quinolin-5-yl)carbamothioyl)benzamide (**5**; 0.18 g, 0.479 mmol, 79.50%). Sodium methoxide (NaOMe) (2 equivalent, 0.08 g, 1.598 mmol) was then added to the stirred solution *N*-((3-(trifluoromethyl) quinolin-5-yl)carbamothioyl) benzamide (0.30 g, 0.799 mmol) in methanol (MeOH, 10 mL) and stirred at room temperature for 1 h. Upon completion (monitored by TLC), the mixture was concentrated under reduced pressure and diluted with EtOAc and H_2O. The organic layer was separated, washed with brine, and concentrated under reduced pressure. The crude was then

Open Access Article. Published on 04 December 2024. Downloaded on 10/25/2025 4:52:21 AM.
This article is licensed under a Creative Commons Attribution-NonCommercial 3.0 Unported Licence.

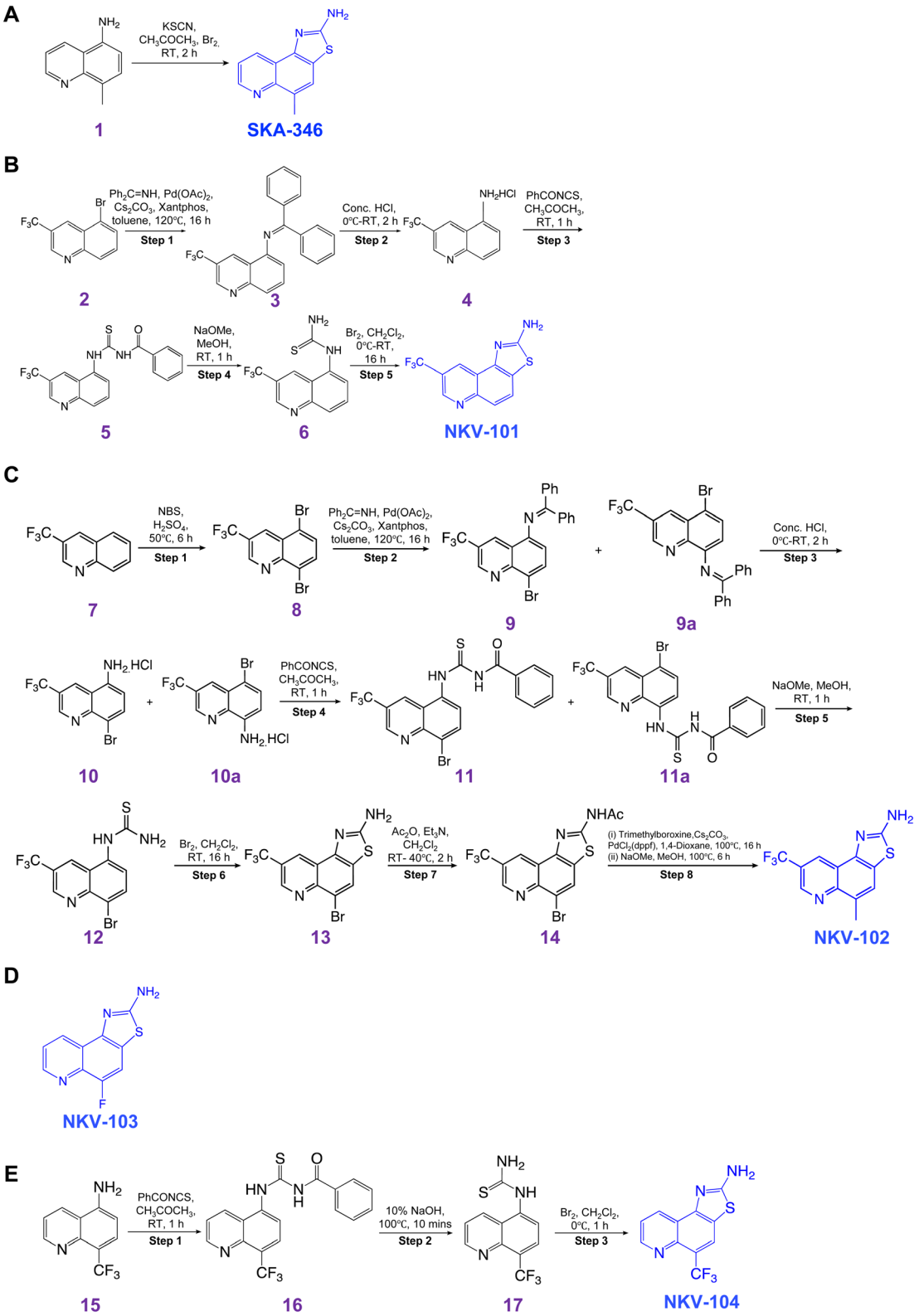

Scheme 1

purified by combi-flash column chromatography (30–50% EtOAc/hexane) to afford 1-(3-(trifluoromethyl)quinolin-5-yl) thiourea (**6**; 0.20 g, 0.737 mmol, 92.29%). Br_2 (0.10 mL) was then added to a stirred solution of **6** (0.15 g, 0.552 mmol) in dichloromethane (CH_2Cl_2, 10 mL) and stirred at room temperature for 16 h. After completion (monitored by TLC), the

 © 2024 The Author(s). Published by the Royal Society of Chemistry

Open Access Article. Published on 04 December 2024. Downloaded on 10/25/2025 4:52:21 AM.
This article is licensed under a Creative Commons Attribution-NonCommercial 3.0 Unported Licence.

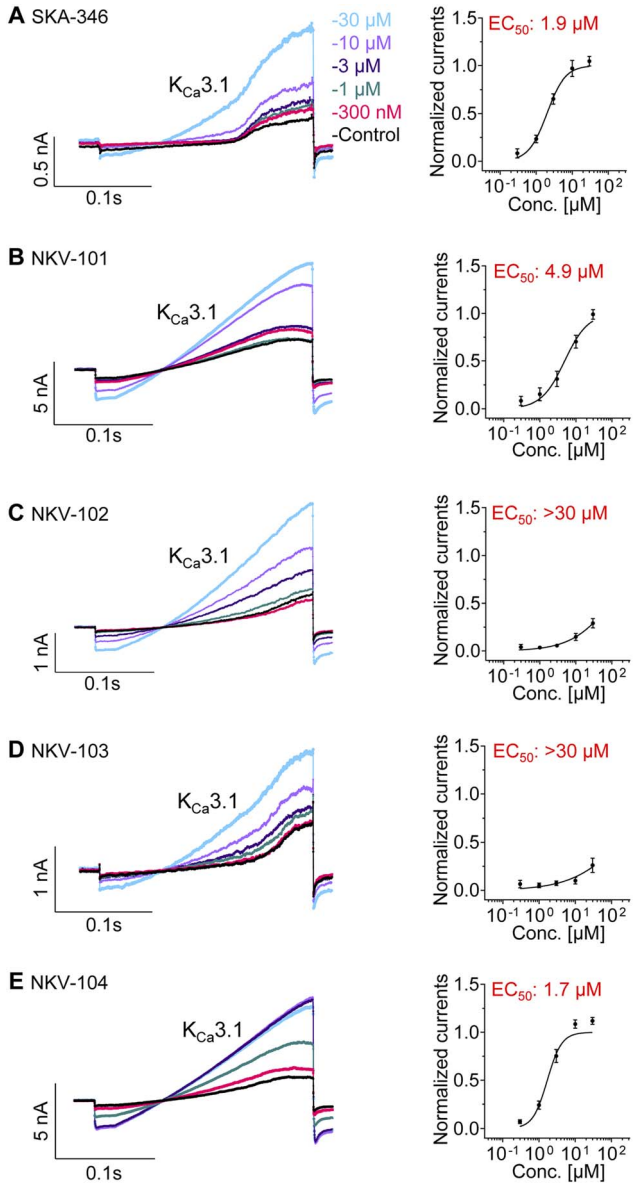

Fig. 1 Patch-clamp recordings of the five quinoline derivatives in activating $K_{Ca}3.1$ channel. Representative current recordings and concentration response curves of the five quinoline derivatives towards the $K_{Ca}3.1$ channel are shown in the left and right columns, respectively; (A) SKA-346, (B) NKV-101, (C) NKV-102, (D) NKV-103, (E) NKV-104. Concentrations of each quinoline derivatives (between 300 nM to 30 μM) were log transformed and plotted against the normalized current values derived from at least three individual cells to generate the concentration–response curves. The EC_{50} values in activating $K_{Ca}3.1$ were computationally determined *via* GraphPad Prism v10.1.2. EC_{50}, effective concentration 50%; EC_{50}: >30 μM, EC_{50} could not be achieved at the highest tested concentration of 30 μM. Data are mean ± SEM of at least three independent experiments.

mixture was quenched in ice-cold H_2O. The organic layer was separated, washed with brine, and concentrated under reduced pressure. The crude was purified by combi-flash column chromatography (50–80% EtOAc/hexane) to afford 8-(trifluoromethyl)thiazolo[4,5-*f*]quinolin-2-amine (**NKV-101**; 0.06 g, 0.222 mmol, 40.32%) as a brown solid. LC-MS calculated for $C_{11}H_6F_3N_3S$: 269.02; found: 270 (M^{+1}); ^1H NMR (400 MHz, DMSO-d_6) δ ppm 9.13 (d, J = 2.25 Hz, 1H), 8.93–8.95 (m, 1H), 8.27 (d, J = 8.88 Hz, 1H), 7.96 (s, 2H), 7.78 (d, J = 8.88 Hz, 1H) (ESI Fig. 2†).

2.1.3. Synthesis of NKV-102. **NKV-102** was synthesized in an 8-steps reaction process (Scheme 1C). Briefly, 3-(trifluoromethyl)quinoline (**7**; 1.80 g, 9.129 mmol), in a stirred solution with sulfuric acid (H_2SO_4, 7 mL) was mixed with *N*-bromosuccinimide (NBS, 1.5 equivalent, 2.43 g, 13.694 mmol) and stirred at 50 °C for 6 h. After completion (monitored by TLC), the mixture was quenched with ice-cold H_2O (50 mL) and extracted with EtOAc (2 × 100 mL). The organic layer was washed with brine (30 mL), dried over anhydrous Na_2SO_4 and concentrated under reduced pressure. The crude was purified by combi-flash column chromatography (30% EtOAc/hexane) to afford 5,8-dibromo-3-(trifluoromethyl)quinoline (**8**; 0.70 g, 1.972 mmol, 21.60%). $Ph_2C{=}NH$ (0.8 equivalent, 0.28 g, 1.577 mmol) and Cs_2CO_3 (2 equivalent, 1.28 g, 3.944 mmol) was then added to a stirred solution of **8** (0.70 g, 1.972 mmol) in toluene (8 mL). The reaction mixture was degassed with argon for 10 min prior to the addition of $Pd(OAc)_2$ (0.2 equivalent, 0.08 g, 0.394 mmol) and Xantphos (0.4 equivalent, 0.45 g, 0.788 mmol). The reaction mixture was then stirred at 120 °C for 16 h. After completion (monitored by TLC), the mixture was quenched with ice-cold H_2O (10 mL) and extracted with EtOAc (2 × 50 mL) and washed with brine (10 mL). The organic layer was dried over anhydrous Na_2SO_4 and concentrated under reduced pressure. The crude was purified by combi-flash column chromatography (70% EtOAc/Heptane) to afford mixture of *N*-(8-bromo-3-(trifluoromethyl)quinolin-5-yl)-1,1-diphenylmethanimine (**9**) and *N*-(5-bromo-3-(trifluoromethyl)quinolin-8-yl)-1,1-diphenylmethanimine (**9a**; 0.70 g, 1.537 mmol, 77.98%). In a mixture of **9** and **9a** (0.70 g, 1.537 mmol) stirred in concentrated HCl (6 mL) at 0 °C, the reaction mixture was left to be stirred at room temperature for 2 h. Upon completion (monitored by TLC), the mixture was quenched with ice-cold H_2O (5 mL) and extracted with EtOAc (2 × 10 mL). The aqueous layer was basified with saturated $NaHCO_3$ (pH 8), washed with brine, dried over anhydrous Na_2SO_4 and concentrated under reduced pressure to afford mixture of 8-bromo-3-(trifluoromethyl) quinolin-5-amine hydrochloride (**10**) and 5-bromo-3-(trifluoromethyl)quinolin-8-amine hydrochloride (**10a**; 0.30 g, 0.915 mmol, 59.58%, HCl salt). PhCONCS (1 equivalent, 0.14 g, 0.915 mmol) was then added to the stirred solution of **10** and **10a** (0.30 g, 0.915 mmol) in CH_3COCH_3 (10 mL). Following which, the reaction mixture was stirred at room temperature for 1 h. After completion (monitored by TLC), the mixture was diluted with EtOAc and H_2O. The organic layer was separated, washed with brine and concentrated under reduced pressure. The crude was purified by combi-flash column chromatography (30–50% EtOAc/hexane) to afford mixture of *N*-((8-bromo-3-(trifluoromethyl)quinolin-5-yl)carbamothioyl)benzamide (**11**) and *N*-((5-bromo-3-(trifluoromethyl)quinolin-8-yl)carbamothioyl)benzamide (**11a**; 0.40 g, 0.880 mmol, 96.15%). In a stirred solution of mixture of **11** and **11a**; (0.40 g, 0.880 mmol) in MeOH (10 mL), NaOMe (2 equivalent, 0.09 g, 1.761 mmol) was added to it and stirred at room temperature for 1 h. Upon completion

Open Access Article. Published on 04 December 2024. Downloaded on 10/25/2025 4:52:21 AM.
This article is licensed under a Creative Commons Attribution-NonCommercial 3.0 Unported Licence.

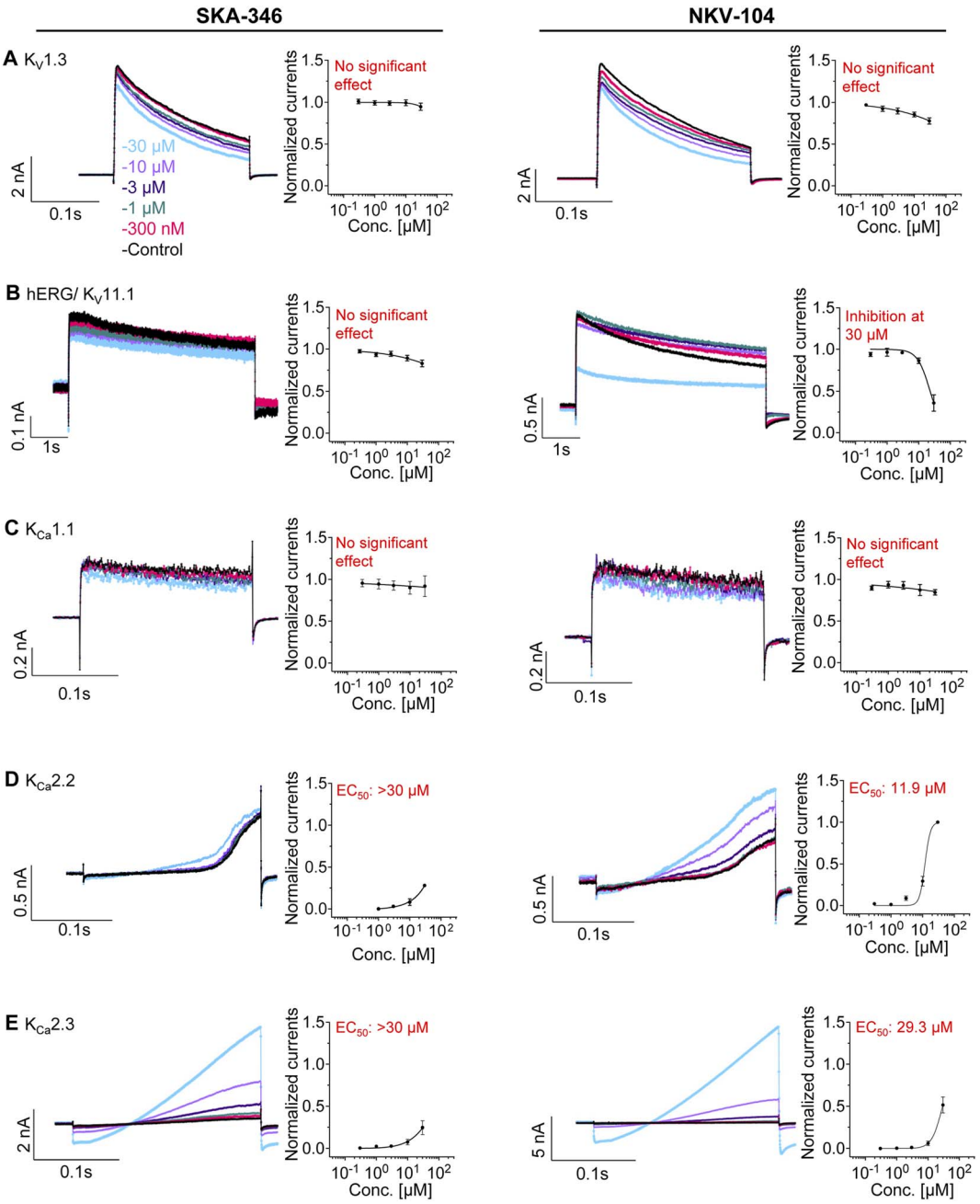

Fig. 2 Patch-clamp recordings of **SKA-346** and **NKV-104** selectivity in activating various K^+ channels. Representative current recordings and concentration response curves of **SKA-346** and **NKV-104** for various K^+ channels are shown in the left and right columns, respectively; (A) K_V1.3, (B) hERG/K_V11.1, (C) K_{Ca}1.1, (D) K_{Ca}2.2, and (E) K_{Ca}2.3. For testing of activation effect, each cell served as its own maximal control and the increases in cell conductance were normalized to the effect obtained with a saturating activator concentration (30 μM **SKA-346**/**NKV-104**) applied during the last liquid periods before the final washout. For channels that were not activated by quinoline derivatives, cell currents were normalized to the last vehicle period applied to the cell. Increasing concentrations of **SKA-346** and **NKV-104** were log transformed and plotted against the normalized current values derived from at least three individual cells to generate the concentration–response curves. Note: **NKV-104**, at a concentration of 30 μM, caused inhibition to K_V11.1 current. EC_{50}, effective concentration 50%. EC_{50}: >30 μM, EC_{50} could not be achieved at the highest tested concentration of 30 μM. Data are mean ± SEM of at least three independent experiments.

(monitored by TLC), the mixture was concentrated under reduced pressure and diluted with EtOAc and H_2O. The organic layer was separated, washed with brine and concentrated under reduced pressure to afford the crude. The crude was then purified by combi-flash column chromatography (30–50% EtOAc/hexane) to yield 1-(8-bromo-3-(trifluoromethyl)quinolin-5-yl)thiourea (**12**; 0.30 g, 0.856 mmol, 97.30%) which was directly used in the next step without purification. Br_2 (0.20 mL) was added to the stirred solution of **12** (0.30 g, 0.856 mmol) in CH_2Cl_2 (10 mL) and stirred at room temperature for 16 h. After

 © 2024 The Author(s). Published by the Royal Society of Chemistry

Open Access Article. Published on 04 December 2024. Downloaded on 10/25/2025 4:52:21 AM.
This article is licensed under a Creative Commons Attribution-NonCommercial 3.0 Unported Licence.

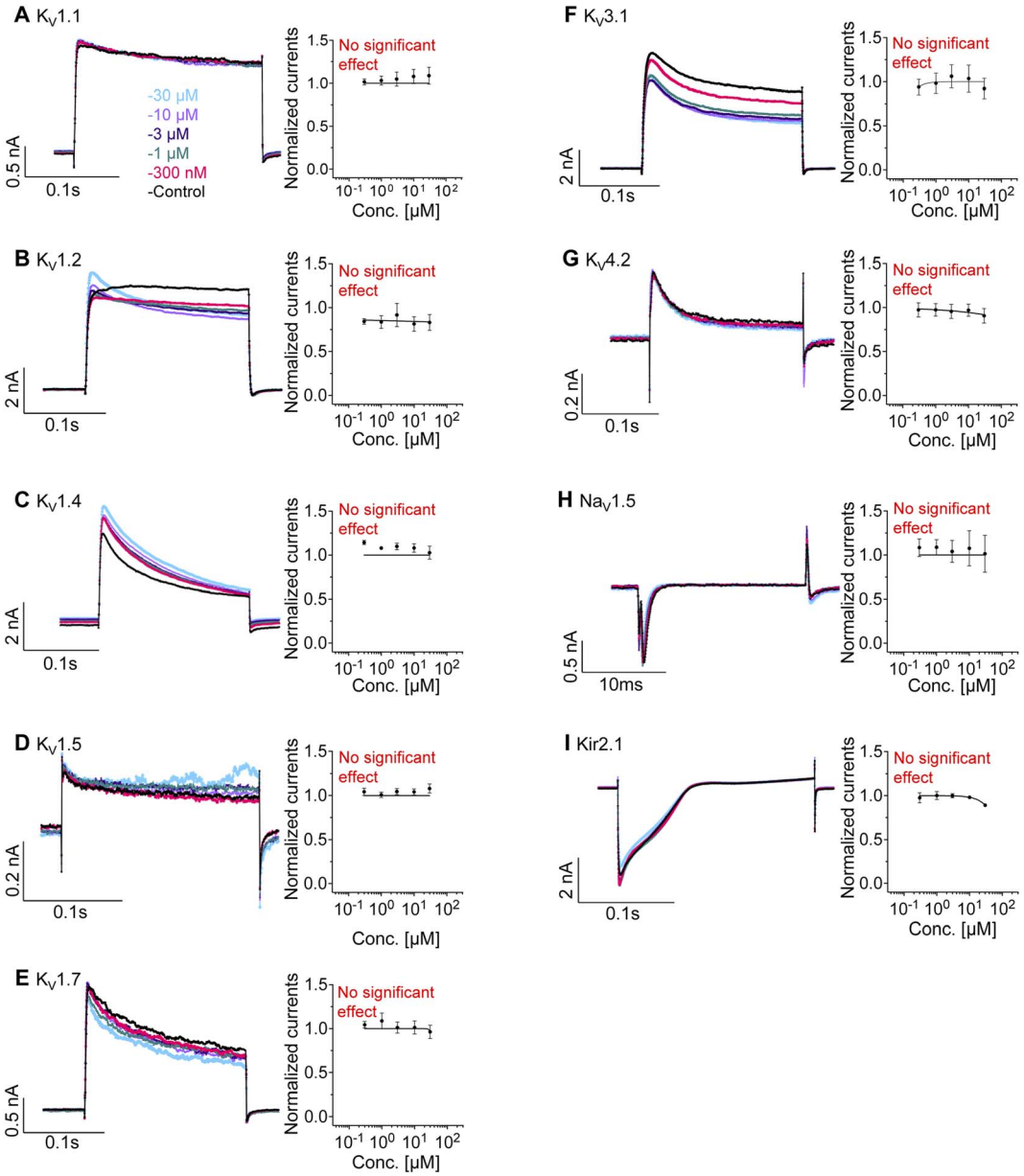

Fig. 3 Patch-clamp recordings of **SKA-346** selectivity in activating various ion channels. Representative current recordings and concentration response curves of **SKA-346** towards 9 different ion channels are shown in the left and right columns, respectively. (A) $K_V1.1$, (B) $K_V1.2$, (C) $K_V1.4$, (D) $K_V1.5$, (E) $K_V1.7$, (F) $K_V3.1$, (G) $K_V4.2$, (H) $Na_V1.5$, and (I) Kir2.1. Concentrations of **SKA-346** (between 300 nM to 30 μM) were log transformed and plotted against the normalized current values derived from at least three individual cells to generate the concentration–response curves. Note: **SKA-346** did not significantly affect any of the tested channels. Data are mean ± SEM of at least three independent experiments.

completion (monitored by TLC), the mixture was quenched with ice-cold H_2O and diluted with CH_2Cl_2. The organic layer was separated, washed with brine and concentrated under reduced pressure. The crude was purified by combi-flash column chromatography (50–80% EtOAc/hexane) to afford 5-bromo-8-(trifluoromethyl)thiazolo[4,5-*f*]quinolin-2-amine (**13**; 0.12 g, 0.344 mmol, 40.24%). Triethylamine (Et_3N) (5 equivalent, 0.30 mL, 2.154 mmol) and acetic anhydride (Ac_2O) (3 equivalent, 0.12 mL, 1.292 mmol) were then added to the stirred solution of **13** (0.15 g, 0.430 mmol) in CH_2Cl_2 (10 mL) at room temperature and stirred at 40 °C for 2 h. After completion (monitored by TLC), the mixture was concentrated under reduced pressure and diluted with CH_2Cl_2 and H_2O. The organic layer was separated and concentrated under reduced pressure. The crude was purified by combi-flash column chromatography (70–80% EtOAc/hexane) to afford *N*-(5-bromo-8-(trifluoromethyl)thiazolo[4,5-*f*]quinolin-2-yl)acetamide (**14**; 0.11 g, 0.281 mmol, 65.43%). Trimethylboroxine (4 equivalent, 0.14 g, 1.127 mmol) and Cs_2CO_3 (2 equivalent, 2.93 g, 9.021 mmol) were then added to the stirred solution of **14** (0.11 g, 0.281 mmol) in 1,4-dioxane (5 mL) and degassed with argon for 5 min prior to the addition of $PdCl_2$ (dppf) (0.1 equivalent, 0.02 g, 0.028 mmol). The reaction

Open Access Article. Published on 04 December 2024. Downloaded on 10/25/2025 4:52:21 AM.
This article is licensed under a Creative Commons Attribution-NonCommercial 3.0 Unported Licence.

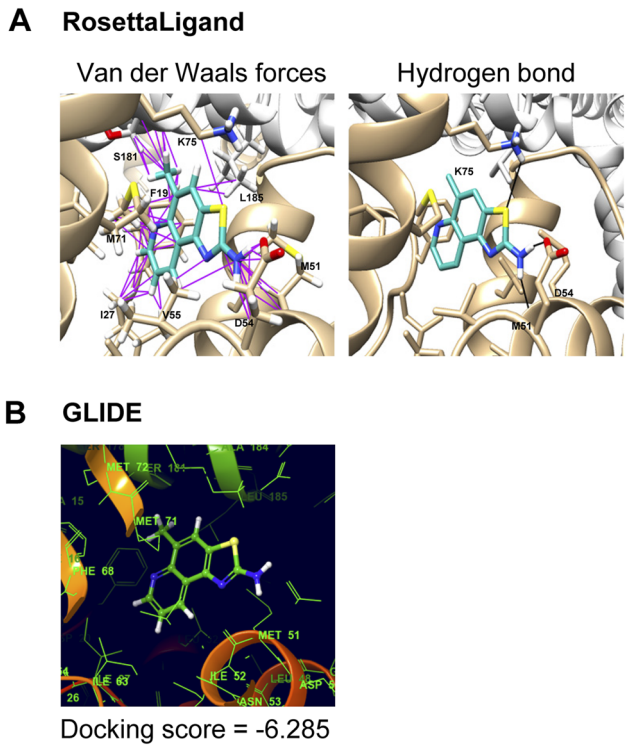

Fig. 4 *In silico* analysis of the docking and binding affinities of **SKA-346** to the binding site of $K_{Ca}3.1$. (A) RosettaLigand docking models of the lowest energy-binding poses of **SKA-346** in the binding site of $K_{Ca}3.1$. Van der Waals forces and hydrogen bonds of the quinoline derivative upon docking within the binding site of $K_{Ca}3.1$ are shown in the left and right columns, respectively. (B) **SKA-346** was prepared in Schrodinger ligand prep Wizard and XP (extra precision) module prior to *in silico* analysis by GLIDE. The binding affinity between **SKA-346** and the binding site of $K_{Ca}3.1$ are computationally predicted that gives an arbitrary number as a docking score, whereby a more negative value suggests a more 'nature-like' fitting of the quinoline derivative within the binding site.

mixture was then stirred at 100 °C for 16 h before it was diluted with EtOAc and H_2O. The organic layer was separated and concentrated under reduced pressure. The crude was dissolved in MeOH (2 mL) followed by the addition of NaOMe (1.5 equivalent, 0.02 g, 0.422 mmol) and stirred at 100 °C for 16 h. After completion (monitored by TLC), the mixture was concentrated under reduced pressure, quenched with ice-cold H_2O, and extracted with EtOAc (2 × 10 mL). The organic layer was separated and concentrated under reduced pressure. The crude was purified by combi-flash column chromatography (70% EtOAc/hexane) to afford 5-methyl-8-(trifluoromethyl)thiazolo[4,5-*f*]quinolin-2-amine (**NKV-102**; 0.013 g, 0.045 mmol, 16.28%) as a solid. LC-MS calculated for $C_{12}H_8F_3N_3S$: 283.04; found: 284.10 (M^{1+}); ^{1}H NMR (400 MHz, DMSO-d_6) δ ppm 9.18 (d, $J = 2.32$ Hz, 1H), 8.93 (d, $J = 1.34$ Hz, 1H), 8.15 (s, 1H), 7.84 (s, 2H), 2.73 (s, 3H) (ESI Fig. 3†).

2.1.4. Synthesis of NKV-103. 5-Fluoro-[1,3]thiazolo[4,5-*f*]quinolin-2-amine, CAS No. 1082821-76-8, **NKV-103** (Scheme 1D) was purchased from ChemSpace (USA) (ESI Fig. 4†).

2.1.5. Synthesis of NKV-104. The synthesis of **NKV-104** was achieved in a 3-steps reaction process (Scheme 1E). With 8-(trifluoromethyl)quinolin-5-amine (**15**; 0.25 g, 1.178 mmol) as the base substrate in CH_3COCH_3 (10 mL), PhCONCS (2 equivalent, 0.38 g, 2.356 mmol) was added to the mixture and stirred at room temperature for 1 h. Upon completion (monitored by TLC), the mixture was diluted with EtOAc and H_2O. The organic layer was separated and concentrated under reduced pressure. The crude was purified by combi-flash column chromatography (40–60% EtOAc/hexane) to afford *N*-((8-(trifluoromethyl)quinolin-5-yl)carbamothioyl)benzamide (**16**; 0.32 g, 0.852 mmol, 72.36%). Compound **16** (0.32 g, 0.852 mmol) was then stirred in 10% NaOH (20 mL) and stirred at 100 °C for 10 min. After completion (monitored by TLC), the mixture was neutralized with $NaHCO_3$ and diluted with EtOAc and H_2O. The organic layer was separated and concentrated under reduced pressure to afford 1-(8-(trifluoromethyl)quinolin-5-yl)thiourea (**17**; 0.18 g, 0.663 mmol, 77.85%) which was directly used in the next step without purification. Br_2 (0.20 mL) was then added to the stirred solution of stirred solution of **17** (0.18 g, 0.663 mmol) in CH_2Cl_2 (10 mL) and stirred at 0 °C for 1 h. Upon completion (monitored by TLC), the mixture was quenched with ice-cold H_2O and diluted with CH_2Cl_2 and H_2O. The organic layer was separated, washed with brine, and concentrated under reduced pressure to afford the crude. The crude was purified by combi-flash column chromatography (50–80% EtOAc/hexane) to afford 5-(trifluoromethyl)thiazolo[4,5-*f*]quinolin-2-amine (**NKV-104**; 0.06 g, 0.222 mmol, 33.59%) as an off-white solid. LC-MS calculated for $C_{11}H_6F_3N_3S$: 269.02; found: 269.70 (M^{+1}); ^{1}H NMR (400 MHz, DMSO-d_6) δ ppm 8.98 (dd, $J = 4.22$, 1.77 Hz, 1H), 8.76 (dd, $J = 8.44$, 1.83 Hz, 1H), 8.58 (s, 1H), 8.14 (s, 2H), 7.66 (dd, $J = 8.38$, 4.22 Hz, 1H) (ESI Fig. 5†).

2.2. Electrophysiology analysis identifies SKA-346 and NKV-104 as potential $K_{Ca}3.1$ activators

Using an automated QPatch-HTX electrophysiology platform (Sophion Biosciences), we performed initial screening of all five quinoline derivatives for their potential activity on the $K_{Ca}3.1$ channel (Fig. 1). Two of the five quinoline derivatives, **SKA-346** and **NKV-104**, augmented $K_{Ca}3.1$ currents with EC_{50} values 1.9 μM and 1.7 μM, respectively (Fig. 1A and E). We therefore prioritized these two compounds for more extensive characterization.

2.3. SKA-346 shows selectivity for the $K_{Ca}3.1$ channel

There are multiple K^+ and other ion channels that are differentially expressed on various cell types and tissues.[24] Non-specific activation of ion channels may lead to potential detrimental side effects, underscoring the need for drug selectivity testing. We therefore examined **SKA-346** and **NKV-104** on three closely related calcium-activating K^+ channels [$K_{Ca}1.1$, expressed mainly in brain, smooth muscle, and skeletal muscle cells; $K_{Ca}2.2$, expressed mainly in neuronal and skeletal muscle cells; and $K_{Ca}2.3$, expressed mainly in neurons and vascular endothelial cells] and two voltage-gated K^+ channels [$K_V1.3$, expressed in T-cells and various immune cell types including

 © 2024 The Author(s). Published by the Royal Society of Chemistry

Open Access Article. Published on 04 December 2024. Downloaded on 10/25/2025 4:52:21 AM.
This article is licensed under a Creative Commons Attribution-NonCommercial 3.0 Unported Licence.

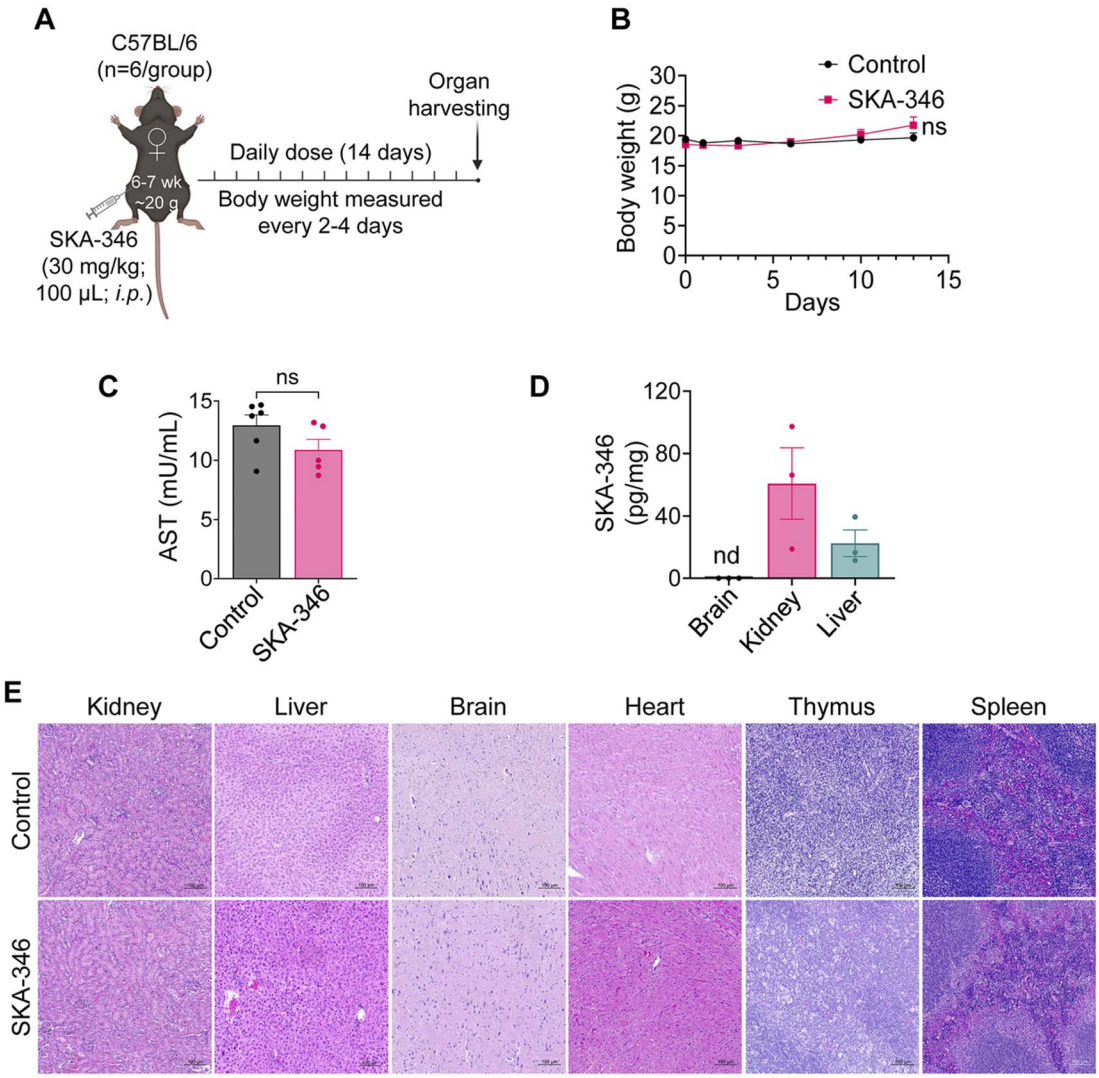

Fig. 5 *In vivo* tolerability of **SKA-346**. **SKA-346** solution was prepared in 3% DMSO + 97% peanut oil to achieve 6 mg mL^{-1} concentration. (A) Timeline of **SKA-346** toxicity studies. **SKA-346** (30 mg kg^{-1}, total volume 100 µL) was administered daily into female C57BL/6 mice ($n = 6$ for each group) *via* i.p. for 14 days. (B) Body weights of control and **SKA-346**-treated mice recorded every 2–4 days. (C) The serum biochemical indicator ast (mU/mL) of control and **SKA-346**-treated mice. (D) Mice brain, kidney, and liver tissues were harvested upon termination and analysed for **SKA-346** biodistribution by LC-MS. (E) H&E staining of mice tissue samples (kidney, liver, brain, heart, thymus, and spleen) harvested upon termination at day 14. Representative images are shown. The full images of the tissue sections are provided as ESI Fig. 9–14.† H&E, hematoxylin and eosin; i.p., intraperitoneal; LC-MS, liquid chromatography-mass spectrometry; nd, not detected; ns, non-significant.

macrophages; and hERG/K_V11.1, a cardiac channel required for the assessment of cardiac safety][25] (Fig. 2A–E). **NKV-104**, at a concentration of 30 µM, inhibited the hERG/K_V11.1 channel (Fig. 2B, right panel) and activated the K_{Ca}2.2 and K_{Ca}2.3 channels with EC_{50} values of 11.9 µM and 29.3 µM, respectively (Fig. 2D and E, right panels), showing its lack of selectivity towards K_{Ca}3.1. **SKA-346** did not activate any of the above channels (Fig. 2, left panels), highlighting its selectivity for K_{Ca}3.1. We therefore focused **SKA-346** for further analysis.

Finally, we tested **SKA-346** on 9 additional ion channels – (1) K_V1.1, expressed in brain, heart, smooth muscle and distal convoluted tubule; (2) K_V1.2, expressed in neurons; (3) K_V1.4, expressed in brain, heart and pancreatic β-cells; (4) K_V1.5, expressed in heart, brain, smooth muscle and pancreatic β-cells; (5) K_V1.7, expressed in neuronal adrenal gland, brain and smooth muscle cells; (6) K_V3.1, expressed in neuronal cells; (7) K_V4.2, expressed in the heart and in neurons; (8) Na_V1.5 expressed in heart, neurons, and skeletal muscle cells; and (9) Kir2.1 expressed in smooth muscle, neurons and endothelial cells.[24] **SKA-346** did not impact any of these ion channels at concentrations up to 30 µM (Fig. 3), confirming its selectivity towards K_{Ca}3.1 channel over 14 other ion channels.

2.4. Molecular docking of SKA-346

The interface between the calmodulin N-lobe and the S_{45}A helix in the S4–S5 linker of K_{Ca}3.1 is intimately involved in Ca^{2+}-calmodulin-dependent activation of the K_{Ca}3.1 channel and has been suggested to be a binding pocket for activators of the

Open Access Article. Published on 04 December 2024. Downloaded on 10/25/2025 4:52:21 AM.
This article is licensed under a Creative Commons Attribution-NonCommercial 3.0 Unported Licence.

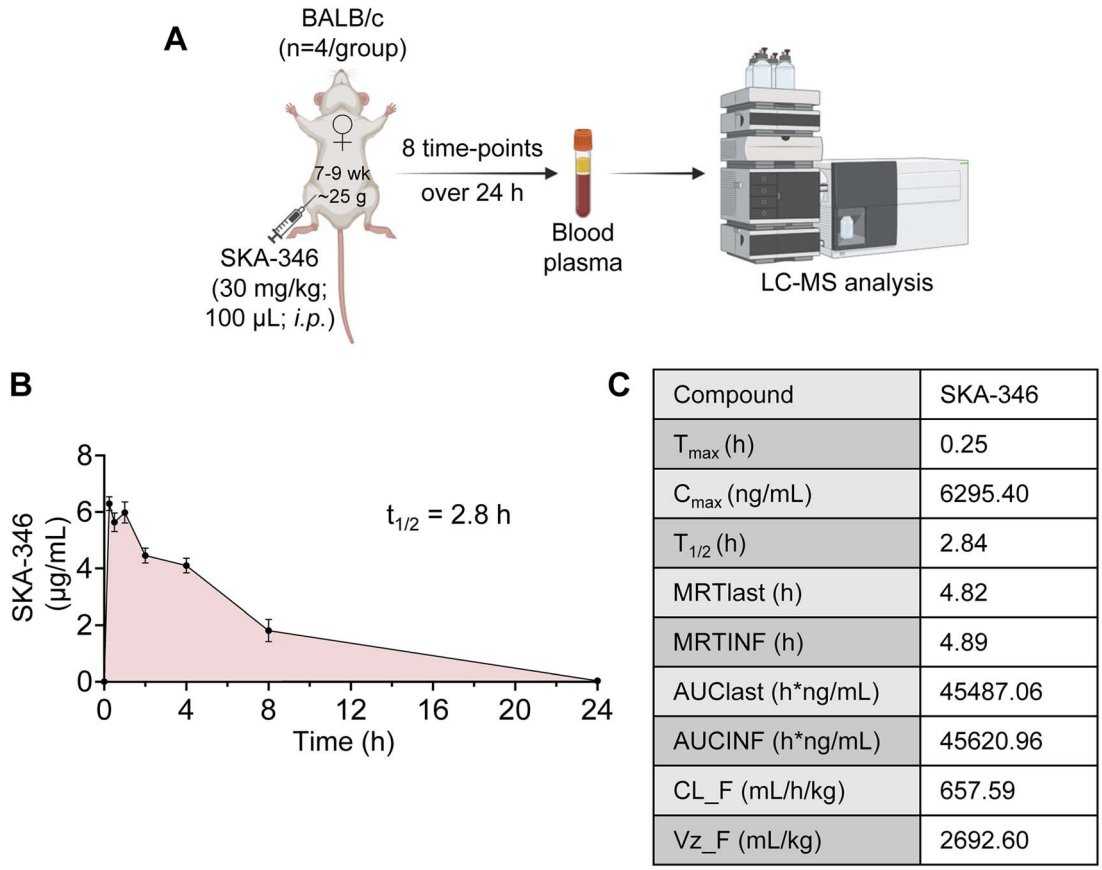

Compound	SKA-346
T_{max} (h)	0.25
C_{max} (ng/mL)	6295.40
$T_{1/2}$ (h)	2.84
MRTlast (h)	4.82
MRTINF (h)	4.89
AUClast (h*ng/mL)	45487.06
AUCINF (h*ng/mL)	45620.96
CL_F (mL/h/kg)	657.59
Vz_F (mL/kg)	2692.60

Fig. 6 *In vivo* pharmacological analysis of **SKA-346**. **SKA-346** solution was prepared in 3% DMSO + 97% peanut oil to achieve 6 mg mL^{-1} concentration. (A) Workflow of **SKA-346** treatment and sample collection over 24 h. Female BALB/c mice (n = 4/group, 2 groups) were administered at 30 mg kg^{-1}; 100 µL of **SKA-346** preparation *via* i.p. Blood plasma was taken from each group of mice alternately at 8 different time-points over the course of 24 h; 0 h, 0.25 h, 0.5 h, 1 h, 2 h, 4 h, 8 h, and 24 h. (B) **SKA-346** concentrations in the mice blood plasma, as determined by LC-MS, were plotted against time over a period of 24 h. The circulating half-life ($t_{1/2}$) of **SKA-346** was calculated to be 2.8 h. (C) Key pharmacological parameters obtained from **SKA-346**-treated mice are tabulated. Detailed list of pharmacological parameters is provided as ESI Table 1.† i.p., intraperitoneal; LC-MS, liquid chromatography-mass spectrometry.

channel.[25,26] **SKA-346** was docked into this critical pocket *via* RosettaLigand computer-aided docking.[27,28] Ligand docking using the RosettaLigand method involves three stages. First, the ligand is randomly placed within a 10 Å sphere of the binding site. Conformers are generated and scored for shape compatibility with the protein, and the best models are filtered and selected for further stages. In the second stage, the ligand's position and orientation are fine-tuned using Monte Carlo minimization, with protein side chains repacked and optimized. The full-atom Rosetta energy function, including softened van der Waals interactions, is used for scoring. The final stage applies a stricter gradient-based minimization with a hard-repulsive van der Waals potential to refine the ligand and protein interactions, improving discrimination between native and non-native binding modes.[29,30] A total of 10 000 models were generated, taken through the above three stages of RosettaLigand docking, followed by the selection of the top 1000 models that attained the lowest total energy score. The models were further sieved to identify the top 10 models which were inspected for ligand/channel interaction and convergence. RosettaLigand predicted a single, well-converged pose for **SKA-346** (Fig. 4A).

We next performed a secondary *in silico* analysis *via* the GLIDE program (open state −1, pdb: 6CNN) that empirically predicts the binding affinity between the compound and binding site upon docking. For this, **SKA-346** was prepared in Schrodinger ligand prep Wizard and XP (extra precision) module (Schrödinger, Inc.). Various orientations of **SKA-346** inputted into the binding pocket in the calmodulin/$K_{Ca}3.1$ interface were computationally determined and labelled as a docking score (Fig. 4B). We found a high negative docking score of −6.285, suggesting a 'nature-like' fitting of **SKA-346** within the binding site.

2.5. Preclinical pharmacology of SKA-346

To access preclinical pharmacology of **SKA-346**, we first characterized its physicochemical properties by using pkCSM (**https://biosig.lab.uq.edu.au/pkcsm**)[31] and Chemdraw 22.2.0. **SKA-346**, molecular formula $C_{11}H_9N_3S$, has a molecular weight of 215.27 g mol^{-1} with calculated partition coefficient

 © 2024 The Author(s). Published by the Royal Society of Chemistry

Open Access Article. Published on 04 December 2024. Downloaded on 10/25/2025 4:52:21 AM. This article is licensed under a Creative Commons Attribution-NonCommercial 3.0 Unported Licence.

(log P) of 2.74 (computed using pkCSM) and 2.53 (computed using Chemdraw 22.2.0). The compound contains 1 hydrogen-bond donor and 4 hydrogen-bond acceptors. The molar refractivity of **SKA-346** is 64.29 with topological polar surface area (TPSA) of 90.579 (computed using pkCSM) and 80.04 (computed using Chemdraw 22.2.0). All these parameters satisfy the generally accepted Lipinski's rule of five,[32] suggesting **SKA-346** to be a drug-like compound. **SKA-346** solubility in dimethyl sulfoxide (DMSO) was calculated to be 40.6 mg mL^{-1} or 188.64 mM (ESI Fig. 6†) Notably, *in vitro* treatment of human primary T-cells (isolated from healthy volunteers' blood using standard protocol)[33] with **SKA-346** concentrations up to 10 μM (~5 times of EC_{50}) were non-cytotoxic (ESI Fig. 7†).

We (co-author Wulff's research group) have previously shown that up to 30 mg kg^{-1} of the benzothiazole compound SKA-31 is well-tolerated in Sprague-Dawley rats and in mice when administered intraperitoneally (i.p.).[22] Using this dataset as a reference and to minimize animal usage, we assessed whether the same single dose of **SKA-346** (30 mg kg^{-1} in 100 μL per animal) administered into female C57BL/6 mice ($n = 6$ each group) *via* i.p. route was tolerated over a short-term period of 14 consecutive days (Fig. 5A). When compared to the vehicle control group, we did not detect any obvious clinical sign of toxicity due to **SKA-346** administration, as there was no significant mouse body weight loss (Fig. 5B). **SKA-346** treatment did not cause any significant change in the levels of serum aspartate aminotransferase (AST, Fig. 5C), indicating that there was no major damage or injury to the liver. AST is a commonly used marker for liver function as any insult or damage to the liver or even skeletal and heart tissues will cause this enzyme to be released into the bloodstream resulting in its significantly elevated levels in the serum.[34] Since the study was designed to provide a preliminary assessment of **SKA-346** safety *in vivo*, we limited our study to a single dose of 30 mg kg^{-1} for 14 consecutive days treatment. It would be important to test both lower and higher doses of **SKA-346** over extended periods and perform assessments using multiple biomarkers to fully characterize potential dose-dependent sub-chronic and chronic toxicity and further establish its safety profile.

LC-MS analysis of harvested organ samples showed substantial amounts of **SKA-346** in the kidney (60.7 pg mg^{-1}) and liver (22.5 pg mg^{-1}), but not in the brain (Fig. 5D). Moreover, the boiled-egg model analysis from SwissADME (**http://www.swissadme.ch**), that utilizes the TPSA and log P values to evaluate the likelihood of the molecule in passing through the blood–brain barrier (BBB),[35] indicated **SKA-346** being unable to cross the BBB (ESI Fig. 8†). It is possible that **SKA-346** distributes into other tissues such as heart, thymus, spleen, lungs, and bones, which could not be analyzed in the current study. When compared to the vehicle control, no detectable change in histological morphologies was observed in vital organs (kidney, liver, heart, brain, thymus, and spleen) of mice due to **SKA-346** administration (Fig. 5E). These findings collectively demonstrate that **SKA-346** did not cause any unwanted toxicity effect to the vital organs.

Finally, we determined the circulating half-life ($t_{1/2}$) of **SKA-346** (30 mg kg^{-1}) administered by i.p. injection in female BALB/c mice ($n = 4$ each). Analysis of blood plasma samples, harvested at multiple time-points over the course of 24 h, by LC-MS (Fig. 6A) revealed that **SKA-346** was absorbed rapidly into the blood, reaching its peak concentration in the blood plasma within 0.25 h (Fig. 6B, ESI Fig. 15†). An estimated circulated half-life ($t_{1/2}$) of **SKA-346** was 2.84 h with the peak plasma concentration (C_{max}) of 6.29 μg mL^{-1} (29.2 μM) at 15 min, which is about 15 times higher than the EC_{50} for $K_{Ca}3.1$ activation. We also noted mean residence time from time of dosing to time of last measurable concentration (MRTlast) to be 4.82 h and the area under the curve from the time of dosing to the time of the last measurable concentration (AUClast) to be 45 487.06 h*ng mL^{-1} (Fig. 6C; ESI Table 1†).

3 Conclusions

In summary, our current study identified **SKA-346** as a novel selective and safe activator of the $K_{Ca}3.1$ channel. **SKA-346** constitutes a promising novel therapeutic for use in conditions that require increasing $K_{Ca}3.1$ activity.

4 Materials and methods

4.1. Ion channel electrophysiology analysis

All the five quinoline derivatives were dissolved in DMSO to prepare 10 mM stock solutions and stored at −80 °C until use. For patch-clamp analysis, fixed-ratio dilutions of the above five compounds were made in extracellular solution buffers, specific for each channel as detailed below. Patch-clamp recordings were captured using an automated QPatch-HTX electrophysiology platform (Sophion Biosciences) equipped with Sophion QPatch software. Each current slope was the average of five measurements taken at the end of the respective liquid period. Data fitting to the Hill equation to obtain EC_{50} values was performed with GraphPad Prism v10.1.2. For testing of activation effect, each cell served as its own maximal control and the increases in cell conductance were normalized to the effect obtained with a saturating activator concentration (30 μM **SKA-346**) applied during the last liquid periods before the final washout.

4.1.1. Patch-clamp of $K_{Ca}3.1$, $K_{Ca}2.2$, and $K_{Ca}2.3$ channels. $K_{Ca}3.1$ and $K_{Ca}2.2$ channels were stably expressed in the human kidney-derived cell line HEK293, and $K_{Ca}2.3$ channels were stably expressed in African green monkey kidney fibroblast-like cell line COS-7.[36] Channel currents were recorded at a holding potential of −80 mV, stepping to −120 mV for 20 ms, then ramping from −120 mV to 40 mV over 200 ms, and stepping back to −120 mV for 20 ms at every 10 seconds interval. The external solution consisted of 160 mM NaCl, 4.5 mM KCl, 1 mM $MgCl_2$, 2 mM $CaCl_2$, 10 mM glucose, and 10 mM HEPES, pH 7.4. The internal buffer contained 120 mM KCl, 5.96 mM $CaCl_2$, 1.75 mM $MgCl_2$, 10 mM EGTA, 10 mM HEPES, and 4 mM Na_2ATP, pH 7.2.

4.1.2. Patch-clamp of $K_V1.3$ and $K_V3.1$ channels. $K_V1.3$ and $K_V3.1$ channels were stably expressed in mouse fibroblast cell line L929.[37] Channel currents were recorded at a holding potential of −90 mV, then depolarized to 40 mV for 200 ms at

Open Access Article. Published on 04 December 2024. Downloaded on 10/25/2025 4:52:21 AM. This article is licensed under a Creative Commons Attribution-NonCommercial 3.0 Unported Licence.

every 45 seconds interval. The external solution consisted of 160 mM NaCl, 4.5 mM KCl, 1 mM $MgCl_2$, 2 mM $CaCl_2$, and 10 mM HEPES, pH 7.2. The internal buffer contained 160 mM KF, 2 mM $MgCl_2$, 10 mM EGTA, and 10 mM HEPES, pH 7.2.

4.1.3. Patch-clamp of $K_V1.1$, $K_V1.4$, $K_V4.2$, $K_V1.2$, and $K_V1.7$ channels. $K_V1.1$ channels were stably expressed in mouse L929 cells, $K_V1.4$ and $K_V4.2$ channels were stably expressed in the mouse cell line LTK, $K_V1.2$ channels were stably expressed in the mouse cell line B82, and $K_V1.7$ channels were stably expressed on the Chinese hamster lung-derived cell line CHL.[37,38] Channel currents were recorded at a holding potential of −80 mV, then depolarized to 40 mV for 200 ms. Interpulse intervals were every 10 seconds for $K_V1.1$ channels, every 15 seconds for $K_V4.2$ channels, and every 30 seconds for $K_V1.4$, $K_V1.2$ and $K_V1.7$ channels. The external solution consisted of 160 mM NaCl, 4.5 mM KCl, 1 mM $MgCl_2$, 2 mM $CaCl_2$, and 10 mM HEPES, pH 7.2. The internal buffer contained 160 mM KF, 2 mM $MgCl_2$, 10 mM EGTA, and 10 mM HEPES, pH 7.2.

4.1.4. Patch-clamp of $K_V1.5$ channels. $K_V1.5$ channels were stably expressed in the murine erythroleukemia MEL cell line.[37] Channel currents were recorded at a holding potential of −80 mV, then depolarized to 60 mV for 200 ms at every 30 seconds interval. The external solution consisted of 160 mM NaCl, 4.5 mM KCl, 1 mM $MgCl_2$, 2 mM $CaCl_2$, and 10 mM HEPES, pH 7.2. The internal buffer contained 160 mM KF, 2 mM $MgCl_2$, 10 mM EGTA, and 10 mM HEPES, pH 7.2.

4.1.5. Patch-clamp of $K_{Ca}1.1$ channels. $K_{Ca}1.1$ channels were stably expressed in human HEK293 cells.[39] Channel currents were recorded at a holding potential of −80 mV, then depolarized to 60 mV for 200 ms at every 10 seconds interval. The external solution consisted of 160 mM NaCl, 4.5 mM KCl, 1 mM $MgCl_2$, 2 mM $CaCl_2$, and 10 mM HEPES, pH 7.4. The internal buffer contained 160 mM KF, 2 mM $MgCl_2$, 10 mM EGTA, and 10 mM HEPES, pH 7.4.

4.1.6. Patch-clamp of hERG/$K_V11.1$ channels. hERG channels were stably expressed in human HEK293 cells (obtained from ICE Bioscience Inc., China). Channel currents were recorded at a holding potential of −80 mV, stepping to −50 mV for 80 ms, then depolarizing to 30 mV for 4.8 seconds, followed by a 5 seconds tail step to −50 mV, and then stepping back to −80 mV for 3.1 seconds at every 15 seconds interval. The external solution consisted of 145 mM NaCl, 4 mM KCl, 1 mM $MgCl_2$, 2 mM $CaCl_2$, 10 mM glucose, and 10 mM HEPES, pH 7.4. The internal buffer contained 115 mM K-Aspartic acid, 20 mM KCl, 1 mM $MgCl_2$, 5 mM EGTA, 10 mM HEPES, and 2 mM Na_2ATP, pH 7.2.

4.1.7. Patch-clamp of Kir2.1 channels. Kir2.1 channels were stably expressed in human HEK293 cells (obtained from ICE Bioscience Inc., China). Channel currents were recorded at a holding potential of −80 mV, stepping to −150 mV for 5 ms, then ramping from −150 mV to 50 mV over 200 ms, and stepping back to −80 mV for 20 ms at every 10 seconds interval. The external solution consisted of 145 mM NaCl, 4 mM KCl, 1 mM $MgCl_2$, 2 mM $CaCl_2$, 10 mM glucose, and 10 mM HEPES, pH 7.4. The internal buffer contained 115 mM K-Aspartic acid, 20 mM KCl, 1 mM $MgCl_2$, 5 mM EGTA, 10 mM HEPES, and 2 mM Na_2ATP, pH 7.2.

4.1.8. Patch-clamp of $Na_v1.5$ channels. $Na_V1.5$ channels were stably expressed in the Chinese hamster epithelial cell line CHO (obtained from ICE Bioscience Inc., China). Channel currents were recorded at a holding potential of −120 mV, depolarized to 0 mV for 20 ms, stepped to a V-half voltage of −70 mV for 8 seconds, followed by stepping back to −120 mV for 20 ms before a depolarizing voltage step to 0 mV for 20 ms, and then back to −120 mV at every 20 seconds interval. The external solution consisted of 145 mM NaCl, 4 mM KCl, 1 mM $MgCl_2$, 2 mM $CaCl_2$, 10 mM glucose, and 10 mM HEPES, pH 7.4. The internal buffer contained 120 mM CsF, 5 mM NaCl, 2 mM $MgCl_2$, 30 mM CsCl, 10 mM EGTA, and 5 mM HEPES, pH 7.2.

4.2. Solubility of SKA-346

SKA-346 solubility in DMSO was determined using UV-Vis spectrophotometer (Varioskan LUX Multimode Microplate Reader, ThermoFisher Scientific, USA), as described earlier.[40] Briefly, **SKA-346** was weighed in a 2 mL glass tube and dissolved in DMSO to achieve a stock concentration of 0.5 mg mL^{-1}. The solution was serially diluted to get concentrations ranging from 0.5 to 0.007 mg mL^{-1}. The absorption spectrum of 200–800 nm showed the absorption peak for **SKA-346** at 345 nm (λ_{max}). Accordingly, a calibration curve was generated by plotting the absorbance at 345 nm (after blank correction) against known concentrations. To determine **SKA-346** solubility, excess amount of **SKA-346** (50 mg) was added to 500 μL DMSO in a 2 mL glass tube, which was then placed on a shaker at 1000 rpm for 24 h to ensure saturation. The suspension was filtered using a 0.22 μm syringe filter to remove undissolved particles and the filtrate was diluted 100-fold in DMSO. The optical density at the absorption peak was used to determine the solubility of **SKA-346** with reference to the calibration curve.

4.3. SKA-346 tolerability assessment in mice

All protocols for animal treatment and care were in accordance with the guidelines for Responsible Care and Use of Laboratory Animals and were reviewed and approved by the Animal Ethics Committee of Singapore Health Services, SingHealth Singapore (IACUC #2018/SHS/1417). DMSO is a polar aprotic solvent that dissolves both polar and nonpolar compounds and is miscible in a wide range of organic solvents, including various oils. For administering **SKA-346** in mice, we dissolved it in 3% DMSO + 97% peanut oil (Sigma-Aldrich, USA) to wet the surface and break up the **SKA-346** crystals to allow for better dissolution of this highly lipophilic compound in peanut oil, as used earlier with a slight modification.[41–43] Goal was to reduce the amount of DMSO to a minimum possible volume. Briefly, peanut oil was heated to a temperature of ∼60 °C in a sterile glass container with a mini-stir bar on a magnetic hotplate stirrer. **SKA-346** in DMSO was added to oil with constant stirring to obtain the final preparation containing 6 mg per mL **SKA-346** (DMSO: peanut oil = 3 : 97). The final **SKA-346** solution was allowed to cool to room temperature, and it appeared light brownish in colour. The **SKA-346** preparation was then aliquoted into autoclaved 2 mL glass vials and stored at −20 °C until use. Prior to injection, the **SKA-346** preparation was thawed, heated to ∼60 °C with stirring and

 © 2024 The Author(s). Published by the Royal Society of Chemistry

Open Access Article. Published on 04 December 2024. Downloaded on 10/25/2025 4:52:21 AM.
This article is licensed under a Creative Commons Attribution-NonCommercial 3.0 Unported Licence.

then cooled to room temperature. Female C57BL/6 mice (aged 6–7 weeks at the start of the treatment, $n = 6$) were injected (i.p.) with ~100 μL of 6 mg mL^{-1} preparation (*i.e.*, 30 mg kg^{-1}) of **SKA-346** once daily for 14 consecutive days. Similarly, control mice ($n = 6$) were injected with a solution of 3% DMSO in 97% peanut oil. Both groups (vehicle and **SKA-346** treated) consisted of mice of similar age and weight ranges to ensure that any observed effects could be attributed primarily to the treatment rather than differences in these biological factors. Mice at the SingHealth facility (Singapore) were housed under standard conditions on a 12 h/12 h light/dark cycle with regulated temperature and humidity and fed with certified standard chow and tap water ad libitum. Mice were monitored daily by trained technicians throughout the study to check any signs of weight loss, intractable diarrhoea, or infection. Body weights were recorded every 2–4 days throughout the experiment. At the end of the treatment on day 14, mice were euthanized, and blood and organs (kidney, liver, brain, heart, thymus, and spleen) were harvested for biochemical and histological analysis.

AST levels in the mice serum samples were determined using commercially available colorimetric kits from Abcam (UK) in accordance with the instructions provided.

Harvested organs were fixed, embedded in paraffin, sectioned, and then mounted on glass slides. Tissue sections slides were placed in a 60 °C incubator for 1 h to remove excess paraffin. The section slides were stained with the histological stains hematoxylin and eosin using Leica ST5010 Autostainer (Leica, Germany). Cover glass slides were mounted onto the H&E-stained tissue sections and dried in the fume hood overnight. Slides were imaged using Zeiss Axioscan 7 microscope slide scanner (Zeiss, Germany) and presented.

4.4. *In vivo* pharmacokinetics profiling

Animal experiments for *in vivo* pharmacokinetics assessments of **SKA-346** were conducted as per the protocol approved by the Animal Ethics Committee of Biological Resource Centre, A*STAR, Singapore (IACUC #201561). Female BALB/c mice (aged 7–9 weeks at the start of the treatment, $n = 4$ for each time-point) were injected intraperitoneally with **SKA-346** at the dose of 30 mg kg^{-1}/10 mL using 3% DMSO + 97% peanut oil formulation. Post-administration of **SKA-346**, blood samples were collected at 0, 0.25, 0.5, 1, 2, 4, 8, and 24 h. Plasma was separated from the blood samples and subsequently analyzed by LC-MS for **SKA-346** quantification.

4.5. LC-MS analysis of SKA-346 in mice blood plasma and organ samples

The LC-MS analysis was performed using Waters equipment coupled with Xevo TQ-S MS system (Waters Corporation, USA). Mice blood plasma samples (20 μL each) were prepared by rapid mixing with 60 μL LC-MS grade methanol: dichloromethane (1 : 1) on a vortex mixer. Tissue samples were prepared by homogenization of pre-weighed organs in 500 μL LC-MS grade methanol: dichloromethane (1 : 1) using a tissue homogenizer. These samples were incubated at 4 °C for 30 min, centrifuged at 14 000 rpm at 4 °C for 10 min, and then injected into LC-MS system for analysis. The UHPLC system was equipped with a BEH C18 column (2.1 mm × 100 mm, 1.7 μm, Waters Corporation, USA). The column temperature was kept at 40 °C. The mice blood plasma and organs samples were eluted at a flow rate of 0.3 mL min^{-1}. Water containing 0.1% formic acid (Solvent A) and acetonitrile containing 0.1% formic acid (Solvent B) were used as mobile phases. For blood plasma samples, the LC was operated with the gradient conditions as follows: 0 min, 20% B; 0.5 min, 20% B; 5 min, 95% B; 7 min, 95% B; 7.1 min, 20% B; 10 min, 20% B. For organ samples, the LC was operated with the gradient conditions as follows: 0 min, 20% B; 5 min, 95% B; 6 min, 95% B; 7 min, 20% B; 10 min, 20% B. The total chromatographic run time was 10 min. Mass spectrometer conditions were set as follows: capillary voltage at 0.5 kV, desolvation temperature at 350 °C, cone gas flow rate at 150 L h^{-1}, desolvation gas flow rate at 800 L h^{-1}, source temperature at 150 °C. The mass spectrometer was operated with an electrospray ionization source (ESI) in the positive mode and performed in the multiple reaction monitoring (MRM) mode. Data acquisition, integration and quantification were performed using MassLynx and TargetLynx (Waters Corporation, USA).

4.6. Statistical analysis

Experiments were replicated independently at least three times. Depending on specific experiments, comparison between two groups was made by paired Student's *t*-test and comparisons of multiple groups within a single experiment were made by one-way ANOVA. Prism 9.5.0 (GraphPad) was used to make the graphs and statistical analyses.

Ethical statement

All animal procedures were performed in accordance with the Guidelines for Responsible Care and Use of Laboratory Animals and as per the protocol approved by the Animal Ethics Committee of Singapore Health Services, SingHealth Singapore (IACUC #2018/SHS/1417) as well as the Biological Resource Centre, A*STAR, Singapore (IACUC #201561). Experiments utilizing human peripheral blood samples were performed in accordance with institutional guidelines and the protocol approved by the Institutional Review Board of Nanyang Technological University Singapore (IRB-2018-05-034).

Data availability

The data supporting this article have been included in the main article and the ESI.†

Author contributions

Conceptualization, B. H. S. W. and N. K. V.; patch clamp analysis, B. H. S. W., S. S. M. G. and S. T. O.; **SKA-346** synthesis, H. W. and H. S.; molecular docking, H. S.; animal experiments, data acquisition and analysis, N. A. B. M. T., K. X. Y. C., K. L., D. H., C. K. O. and T. S. V.; pharmacology, T. S. V., B. H. S. W., D. H. and Y. W.; LC-MS analysis, Y. C. C. and Y. W.; formal analysis, B. H.

Open Access Article. Published on 04 December 2024. Downloaded on 10/25/2025 4:52:21 AM. This article is licensed under a Creative Commons Attribution-NonCommercial 3.0 Unported Licence.

S. W., R. D. W., V. G. S., N. K. V. and H. W.; investigation, B. H. S. W. and N. K. V.; resources, N. K. V. and C. K. O.; data curation, B. H. S. W., S. T. O. and H. S.; writing—original draft, B. H. S. W. and N. K. V.; writing—review & editing, B. H. S. W., S. T. O., D. H., C. K. O., Y. W., H. W., R. D. W., V. G. S. and N. K. V.; supervision, N. K. V., R. D. W. and V. G. S.; project administration, N. K. V.; funding acquisition, N. K. V. All authors have seen and approved the final version of the manuscript.

Conflicts of interest

There is no conflict of interest to declare.

Acknowledgements

Authors acknowledge Professor K. George Chandy for reading, editing, and critiquing this manuscript, and Sai Life Sciences for their help in chemical synthesis. Authors also acknowledge Dr Chang Jun Jie and Dr Loh Xian Jun at Institute of Materials Research and Engineering (IMRE), A*STAR for their assistance in determining the drug solubility. This research was supported, in part, by the Singapore Ministry of Education (MOE) under its MOE Academic Research Fund (AcRF) Tier 2 Grant (MOE2017-T2-2-004), MOE AcRF Tier 1 Grant (RG94/22), and the National Research Foundation Singapore under its Open Fund Large Collaborative Grant (OFLCG-23May0039) and administered by the Singapore Ministry of Health's National Medical Research Council (NMRC). B. H. S. W. was provided with PhD fellowship by HealthTech NTU.

References

1 J. Lam and H. Wulff, The lymphocyte potassium channels $K_v1.3$ and $K_{Ca}3.1$ as targets for immunosuppression, *Drug Dev. Res.*, 2011, **72**, 573–584.

2 S. Ghanshani, H. Wulff, M. J. Miller, H. Rohm, A. Neben, G. A. Gutman, M. D. Cahalan and K. G. Chandy, Up-regulation of the IKCa1 potassium channel during T-cell activation. Molecular mechanism and functional consequences, *J. Biol. Chem.*, 2000, **275**, 37137–37149.

3 P. J. Hanley, B. Musset, V. Renigunta, S. H. Limberg, A. H. Dalpke, R. Sus, K. M. Heeg, R. Preisig-Muller and J. Daut, Extracellular ATP induces oscillations of intracellular Ca^{2+} and membrane potential and promotes transcription of IL-6 in macrophages, *Proc. Natl. Acad. Sci. U.S.A.*, 2004, **101**, 9479–9484.

4 S. M. Duffy, W. J. Lawley, E. C. Conley and P. Bradding, Resting and activation-dependent ion channels in human mast cells, *J. Immunol.*, 2001, **167**, 4261–4270.

5 R. Khanna, L. Roy, X. Zhu and L. C. Schlichter, K^+ channels and the microglial respiratory burst, *Am. J. Physiol.: Cell Physiol.*, 2001, **280**, C796–C806.

6 T. L. Pena and S. G. Rane, The fibroblast intermediate-conductance K_{Ca} channel, FIK, as a prototype for the cell growth regulatory function of the IK channel family, *J. Membr. Biol.*, 1999, **172**, 249–257.

7 R. Kohler, H. Wulff, I. Eichler, M. Kneifel, D. Neumann, A. Knorr, I. Grgic, D. Kampfe, H. Si, J. Wibawa, R. Real, K. Borner, S. Brakemeier, H. D. Orzechowski, H. P. Reusch, M. Paul, K. G. Chandy and J. Hoyer, Blockade of the intermediate-conductance calcium-activated potassium channel as a new therapeutic strategy for restenosis, *Circulation*, 2003, **108**, 1119–1125.

8 C. B. Neylon, R. J. Lang, Y. Fu, A. Bobik and P. H. Reinhart, Molecular cloning and characterization of the intermediate-conductance Ca^{2+}-activated K^+ channel in vascular smooth muscle: relationship between K_{Ca} channel diversity and smooth muscle cell function, *Circ. Res.*, 1999, **85**, e33–e43.

9 J. D. McCann, J. Matsuda, M. Garcia, G. Kaczorowski and M. J. Welsh, Basolateral K^+ channels in airway epithelia. I. Regulation by Ca^{2+} and block by charybdotoxin, *Am. J. Physiol.*, 1990, **258**, L334–L342.

10 I. Grgic, B. P. Kaistha, J. Hoyer and R. Kohler, Endothelial Ca+-activated K^+ channels in normal and impaired EDHF-dilator responses-relevance to cardiovascular pathologies and drug discovery, *Br. J. Pharmacol.*, 2009, **157**, 509–526.

11 L. Sforna, A. Megaro, M. Pessia, F. Franciolini and L. Catacuzzeno, Structure, gating and basic functions of the Ca^{2+}-activated K channel of intermediate conductance, *Curr. Neuropharmacol.*, 2018, **16**, 608–617.

12 M. Zhang, C. Abrams, L. Wang, A. Gizzi, L. He, R. Lin, Y. Chen, P. J. Loll, J. M. Pascal and J. F. Zhang, Structural basis for calmodulin as a dynamic calcium sensor, *Structure*, 2012, **20**, 911–923.

13 M. D. Cahalan and K. G. Chandy, The functional network of ion channels in T lymphocytes, *Immunol. Rev.*, 2009, **231**, 59–87.

14 N. K. Verma, B. H. S. Wong, Z. S. Poh, A. Udayakumar, R. Verma, R. K. J. Goh, S. P. Duggan, V. G. Shelat, K. G. Chandy and N. F. Grigoropoulos, Obstacles for T-lymphocytes in the tumour microenvironment: Therapeutic challenges, advances and opportunities beyond immune checkpoint, *EBioMedicine*, 2022, **83**, 104216.

15 Y. Lin, Y. J. Zhao, H. L. Zhang, W. J. Hao, R. D. Zhu, Y. Wang, W. Hu and R. P. Zhou, Regulatory role of $K_{Ca}3.1$ in immune cell function and its emerging association with rheumatoid arthritis, *Front. Immunol.*, 2022, **13**, 997621.

16 L. Di, S. Srivastava, O. Zhdanova, Y. Ding, Z. Li, H. Wulff, M. Lafaille and E. Y. Skolnik, Inhibition of the K^+ channel $K_{Ca}3.1$ ameliorates T cell-mediated colitis, *Proc. Natl. Acad. Sci. U.S.A.*, 2010, **107**, 1541–1546.

17 C. H. Richards, Z. Mohammed, T. Qayyum, P. G. Horgan and D. C. McMillan, The prognostic value of histological - necrosis in solid organ malignant disease: A systematic review, *Future Oncol.*, 2011, **7**, 1223–1235.

18 R. Eil, S. K. Vodnala, D. Clever, C. A. Klebanoff, M. Sukumar, J. H. Pan, D. C. Palmer, A. Gros, T. N. Yamamoto, S. J. Patel, G. C. Guittard, Z. Yu, V. Carbonaro, K. Okkenhaug, D. S. Schrump, W. M. Linehan, R. Roychoudhuri and N. P. Restifo, Ionic immune suppression within the

 © 2024 The Author(s). Published by the Royal Society of Chemistry

Open Access Article. Published on 04 December 2024. Downloaded on 10/25/2025 4:52:21 AM.
This article is licensed under a Creative Commons Attribution-NonCommercial 3.0 Unported Licence.

tumour microenvironment limits T cell effector function, *Nature*, 2016, **537**, 539–543.

19 S. T. Ong, A. S. Ng, X. R. Ng, Z. Zhuang, B. H. S. Wong, P. Prasannan, Y. J. Kok, X. Bi, H. Shim, H. Wulff, K. G. Chandy and N. K. Verma, Extracellular K^+ dampens T cell functions: implications for immune suppression in the tumor microenvironment, *Bioelectricity*, 2019, **1**, 169–179.

20 A. A. Chimote, A. Balajthy, M. J. Arnold, H. S. Newton, P. Hajdu, J. Qualtieri, T. Wise-Draper and L. Conforti, A defect in $K_{Ca}3.1$ channel activity limits the ability of $CD8^+$ T cells from cancer patients to infiltrate an adenosine-rich microenvironment, *Sci. Signal.*, 2018, **11**, eaaq1616.

21 M. Chirra, H. S. Newton, V. S. Gawali, T. M. Wise-Draper, A. A. Chimote and L. Conforti, How the potassium channel response of T lymphocytes to the tumor microenvironment shapes antitumor immunity, *Cancers*, 2022, **14**, 3564.

22 A. Sankaranarayanan, G. Raman, C. Busch, T. Schultz, P. I. Zimin, J. Hoyer, R. Kohler and H. Wulff, Naphtho[1,2-d]thiazol-2-ylamine (SKA-31), a new activator of $K_{Ca}2$ and $K_{Ca}3.1$ potassium channels, potentiates the endothelium-derived hyperpolarizing factor response and lowers blood pressure, *Mol. Pharmacol.*, 2009, **75**, 281–295.

23 H. Shim, B. M. Brown, L. Singh, V. Singh, J. C. Fettinger, V. Yarov-Yarovoy and H. Wulff, The trials and tribulations of structure assisted design of K_{Ca} channel activators, *Front. Pharmacol*, 2019, **10**, 972.

24 C. Miller, An overview of the potassium channel family, *Genome Biol.*, 2000, **1**, REVIEWS0004.

25 S. D. Harding, J. F. Armstrong, E. Faccenda, C. Southan, S. P. H. Alexander, A. P. Davenport, M. Spedding and J. A. Davies, The IUPHAR/BPS guide to PHARMACOLOGY in 2024, *Nucleic Acids Res.*, 2024, **52**, D1438–D1449.

26 C. Lee and R. Mackinnon, Activation mechanism of a human SK-calmodulin channel complex elucidated by cryo-EM structures, *Science*, 2018, **360**, 508–513.

27 S. A. Combs, S. L. Deluca, S. H. DeLuca, G. H. Lemmon, D. P. Nannemann, E. D. Nguyen, J. R. Willis, J. H. Sheehan and J. Meiler, Small-molecule ligand docking into comparative models with Rosetta, *Nat. Protoc.*, 2013, **8**, 1277–1298.

28 J. Meiler and D. Baker, ROSETTALIGAND: protein-small molecule docking with full side-chain flexibility, *Proteins*, 2006, **65**, 538–548.

29 I. W. Davis and D. Baker, RosettaLigand docking with full ligand and receptor flexibility, *J. Mol. Biol.*, 2009, **385**, 381–392.

30 I. W. Davis, K. Raha, M. S. Head and D. Baker, Blind docking of pharmaceutically relevant compounds using RosettaLigand, *Protein Sci.*, 2009, **18**, 1998–2002.

31 D. E. Pires, T. L. Blundell and D. B. Ascher, pkCSM: Predicting small-molecule pharmacokinetic and toxicity properties using graph-based signatures, *J. Med. Chem.*, 2015, **58**, 4066–4072.

32 C. A. Lipinski, Drug-like properties and the causes of poor solubility and poor permeability, *J. Pharmacol. Toxicol. Methods*, 2000, **44**, 235–249.

33 A. Kizhakeyil, S. T. Ong, M. H. U. T. Fazil, M. L. S. Chalasani, P. Prasannan and N. K. Verma, Isolation of human peripheral blood T-lymphocytes, *Methods Mol. Biol.*, 2019, **1930**, 11–17.

34 J. R. Senior, Alanine aminotransferase: a clinical and regulatory tool for detecting liver injury–past, present, and future, *Clin. Pharmacol. Therapeut.*, 2012, **92**, 332–339.

35 A. Daina, O. Michielin and V. Zoete, SwissADME: a free web tool to evaluate pharmacokinetics, drug-likeness and medicinal chemistry friendliness of small molecules, *Sci. Rep.*, 2017, **7**, 42717.

36 N. Coleman, B. M. Brown, A. Oliván-Viguera, V. Singh, M. M. Olmstead, M. S. Valero, R. Köhler and H. Wulff, New positive Ca^{2+}-activated K^+ channel gating modulators with selectivity for $K_{Ca}3.1$, *Mol. Pharmacol.*, 2014, **86**, 342–357.

37 S. Grissmer, A. N. Nguyen, J. Aiyar, D. C. Hanson, R. J. Mather, G. A. Gutman, M. J. Karmilowicz, D. D. Auperin and K. G. Chandy, Pharmacological characterization of five cloned voltage-gated K^+ channels, types $K_v1.1$, 1.2, 1.3, 1.5, and 3.1, stably expressed in mammalian cell lines, *Mol. Pharmacol.*, 1994, **45**, 1227–1234.

38 C. Beeton, M. W. Pennington, H. Wulff, S. Singh, D. Nugent, G. Crossley, I. Khaytin, P. A. Calabresi, C. Y. Chen, G. A. Gutman and K. G. Chandy, Targeting effector memory T cells with a selective peptide inhibitor of $K_v1.3$ channels for therapy of autoimmune diseases, *Mol. Pharmacol.*, 2005, **67**, 1369–1381.

39 M. R. Tanner, M. W. Pennington, S. S. Chauhan, T. Laragione, P. S. Gulko and C. Beeton, $K_{Ca}1.1$ and $K_v1.3$ channels regulate the interactions between fibroblast-like synoviocytes and T lymphocytes during rheumatoid arthritis, *Arthritis Res. Ther.*, 2019, **21**, 6.

40 R. Kumar and P. F. Siril, Ultrafine carbamazepine nanoparticles with enhanced water solubility and rate of dissolution, *RSC Adv.*, 2014, **4**, 48101–48108.

41 A. Mitrović, J. Završnik, G. Mikhaylov, D. Knez, U. Pečar Fonović, P. Matjan Štefin, M. Butinar, S. Gobec, B. Turk and J. Kos, Evaluation of novel cathepsin-X inhibitors *in vitro* and *in vivo* and their ability to improve cathepsin-B-directed antitumor therapy, *Cell. Mol. Life Sci.*, 2022, **79**, 34.

42 T. Kyllo, V. Singh, H. Shim, S. Latika, H. M. Nguyen, Y. J. Chen, E. Terry, H. Wulff and J. D. Erickson, Riluzole and novel naphthalenyl substituted aminothiazole derivatives prevent acute neural excitotoxic injury in a rat model of temporal lobe epilepsy, *Neuropharmacology*, 2023, **224**, 109349.

43 C. M. John, R. K. Mallat, R. C. Mishra, G. George, V. Singh, J. D. Turnbull, C. S. Umeshappa, D. J. Kendrick, T. Kim, F. M. Fauzi, F. Visser, P. W. M. Fedak, H. Wulff and A. P. Braun, SKA-31, an activator of Ca^{2+}-activated K^+ channels, improves cardiovascular function in aging, *Pharmacol. Res.*, 2020, **151**, 104539.